Full Length Research Paper

Phase and conductivity dynamics of strontium hexaferrite nanocrystals in a hydrogen gas flow

A. A. Fargali[1], M. K. Zayed[2], M. H. Khedr[1]* and A. F. Moustafa[1]

[1]Chemistry Department, Faculty of Science, Beni-Sueif University, Beni-Sueif-62111, Egypt.
[2]Physics Department, Faculty of Science, Beni-Sueif University, Beni-Sueif-62111, Egypt.

The phase and conductivity dynamics of strontium hexaferrite nanocrystals were isothermally studied at different temperatures during a constant flow of hydrogen gas at normal atmospheric pressure. The nanocrystals were prepared by self-flash combustion of acetate precursors. While the formed phase was characterized using XRD, TEM, and optical microscopy after hydrogen exposure, the electrical conductivity was in-situ measured during reduction. The temporal changes in conductivity as well as the formed phases at partial and complete reduction were found to be significantly affected by the operating temperature. Nanocrystals reduced at lower temperatures showed formation of lower oxygen content phases of strontium-iron oxides ($SrFe_{12}O_{19}$, $Sr_2Fe_2O_5$, $Sr_7Fe_{10}O_{22}$), and iron oxides (Fe_3O_4, FeO), while those reduced at higher reducing temperature showed the formation of metallic iron responsible for higher electric conductivity during reduction. Metallic iron nanocrystals of increased sizes were formed at higher reducing temperatures and longer reducing times. Temporal conductivity changes during hydrogen gas flow at different temperatures showed three regions corresponding to removal of surface oxygen, surface reduction, and bulk reduction of the nanocrystals. Nanocrystals reduced at temperatures higher than 400^oC showed three reduction regions corresponding to these mechanisms, whereas those reduced at 400^oC only two regions could be detected. The activation energies of the oxygen desorption, surface reduction and bulk reduction were found to be 55.5, 40.2, and 44.1 kJ mol^{-1} respectively. This indicates that oxygen desorption follows a chemical reaction controlled mechanism, while surface and bulk reductions are of combined gas diffusion and interfacial chemical reaction controlled mechanisms. The results obtained from the conductivity measurements were further supported by thermo-gravimetric measurements.

Key words: Strontium hexaferrite ($SrFe_{12}O_{19}$) nanocrystals, phase changes, electrical conductivity, reduction, thermogravimetric.

INTRODUCTION

Hexaferrites ($MeFe_{12}O_{19}$: Me = Sr, Ba, and Pb) are Industrially important materials that have numerous technological applications such as permanent magnets (Kirchmayr, 1996), microwave devices (Pardavi-Horvath and Magne, 2000), magnetic recording media (Sankaranarayanan et al., 2000), and magneto-optical devices (Gerber, 2000). Appointing for these applications arises from their unique properties of large magnetic crystalline anisotropy, high Curie temperatures, large saturation magnetization and coercive fields, in addition to its mechanical resilient, chemical stability, and low cost (Fu

et al., 2003; Zaitsev et al., 2005). More importantly, their intrinsic magnetic properties can be controlled and modified either by using substitutional metallic elements (Kaura et al., 2006; Licci et al., 1983), controlling size, shape, and size distribution of the particles (Ataie and Heshmati-Manesh, 2001; Hwang et al., 2002), or by special thermal treatment in a reducing gas (Ataie et al., 1996; Ebrahimi et al., 1999; Kitahata and Kishimoto, 1994; Hong et al., 1997). In fact, thermal treatment of hexaferrites in a reducing gas environment modifies the material morphology as well as introducing metallic atoms into the ferrite crystals. For example, a hydrogen atmosphere has been employed to introduce iron into Co-Ti-Sn and Co-Zn-Ti-Sn substituted Ba-ferrite particles by reducing a portion of the Fe ions, thus, an increase in the

---

*Corresponding author. E-mail: dkhedr@yahoo.com.

saturation magnetization was achieved (Kitahata and Kishimoto, 1994; Hong et al., 1997). Heat treatment of strontium hexaferrite (SHF) powders in nitrogen, hydrogen, and carbon atmospheres showed that the phase composition and morphology as well as the magnetic properties are affected significantly by the gas/vapor treatments (Ataie et al., 1996; Ebrahimi et al., 1999).

Based on the composition and oxygen content, strontium ferrite has a number of stable and intermediate phases whose crystal structures and transport properties are considerably affected by oxygen-vacancy ordering (Hodges et al., 2000) While the stoichiometric mono-ferrite, $SrFeO_3$, has a disordered cubic perovskite lattice, a series of structurally distinct vacancy-ordered phases $Sr_nFe_nO_{3n-1}$ $(n = 2, 4, 8)$ is formed with decreasing oxygen partial pressure and oxygen content (Hodges et al., 2000; Prado and Manthiram, 2001; Zainullina et al., 2006). Oxygen defect phases such as $Sr_3Fe_2O_7$, $Sr_3Fe_2O_{6.5}$ and $Sr_3Fe_2O_6$ are antiferromagnetic compounds with semiconductor-like behaviors and thermally activated carriers (Zainullina et al., 2006; Adler, 1999; Shilova et al., 2002; Patrakeev et al., 2001). On the other hand, $Sr_3Fe_2O_{6+\delta}$ and titania-doped derivatives $Sr_3Fe_{2-x}Ti_xO_{6+\delta}$ are mixed ionelectron conductors with an energy gap of 2.3 eV (Zainullina et al., 2006; Adler, 1999; Shilova et al., 2002). Also, the electrical conduction in hexaferrites is a combination of electronic and ionic conduction such that conduction at low temperatures is dominated by electrons whereas at high temperature it is dominated by ionic hopping mechanism (Patrakeev et al., 2001; El-Saadawy, 2000; Seshamma et al., 2006).

It is reported that exposing SHF to static hydrogen gas followed by calcinations in air produced small size particles with improved coercivity and magnetization (Ataie et al., 1996; Ebrahimi et al., 1999). Similar observations were reported for SHF treatment in N_2 and C (Ataie et al., 1996; Ebrahimi et al., 1999). In some cases, an enhancement of about 400% in the SHF coercivity was observed (Ebrahimi et al., 1999). No sufficient information is available on the kinetics of hydrogen reduction on SHF in the bulk or in the nanocrystal forms, neither is the interplayed role between the formed phase and its electric conductivity during reduction. Thus, it is the focus of this work to study the reduction kinetics, phase formation, electric conductivity of SHF nanocrystals during a dynamic hydrogen gas flow at constant atmospheric pressure and different temperatures. The nanocrystals are prepared by self-flash combustion of acetate precursors. In-situ electric measurement is adapted to study the reduction kinetics. X-ray diffraction (XRD) is used for formed phase identifications, while transmission electron microscopy (TEM) and optical microscopy are used to study the morphology of the reduced and partially reduced phases. The chemical behavior is strongly influenced by chemical reaction and are correlated; in the sense that each removal of oxygen atom librates at least two electrons and modifies the conductivity. Therefore, thermo-gravimetric investigations during reduction are used to support the results obtained from in-situ conductivity measurements.

EXPERIMENTAL PROCEDURE

Eight moles of pure fine ferric acetate basic, FeAc, $(CH_3COO)_2Fe.OH$ were well mixed with one mole of strontium acetate, SrAc, $(C_4H_6O_4Sr)$ to insure homogeneity. The mixture was mixed in a beaker containing 150 ml distillated water, heated till water vaporized, then dried at 100^oC for 24 h. The dried powder was then heated vigorously on a hot plate to ensure complete decomposition of acetates and formation of nanocrystal oxides. The nanocrystal powder was moistened with 10% distilled water and equal weights, 1.3 gm, were pressed into cylindrical compacts using cylindrical mould of 1 cm inner diameter and 200 kgm^{-3} applied pressure. A two step drying process, drying at 85^oC for 1 h followed by drying at 100^oC for 24 h, was again used to dry the cylindrical compacts. Single phase SHF nanocrystals were then formed by annealing the dried nanocrystal compacts in a muffle furnace at 850^oC for 45 min.

The electrical conductivity of SHF nanocrystals was measured during hydrogen gas flow (0.5 L min^{-1}). H_2 gas was purified by passing over series of columns filed with silica gel, anhydrous calcium chloride, soda lime and copper turning heated at 500^oC. N_2 gas was used for cleaning the furnace. The electrical conductivity cell was made of two ceramic circular bases joined together by four stainless steel rods. For electrical conductivity measurements, the SHF nanocrystal compacts were mounted between the two stainless steel electrodes and held tightly with the springs. The total resistance, R, of SHF compacts was measured directly using a computerized Avometer. The data is transferred into electrical conductivity (. in cm^{-1}) using the sample geometry ($\sigma = l/(R.A)$), where l is the length and A is the cross-section area.

The reduction kinetic was further investigated using thermo-gravimetric measurements. In this experiment, the oxygen weight loss during hydrogen reduction is measured directly by a digital balance. The reduction kinetics can then be studied by measuring the reduction percentage as a function of time during hydrogen gas flow. The obtained results were then compared with that obtained by in situ conductivity measurements.

The different phases formed during reduction were identified by XRD using JSX-60P JEOL diffractometer. Transmission electron microscopy (TEM) model Joel JSM-1234, and optical microscope are used to study the morphology of the reduced and partially reduced phases.

RESULTS AND DISCUSSION

The conduction behavior of the SHF nanocrystal compact disks was first probed by studying their electrical conductivity-temperature dependence between room temperature and up to the annealing temperature, 850^oC, in air. Figure 1 correlates the DC conductivity of SHF nanocrystal compacts to the temperature during a heating–cooling cycle. The measurements were carried out in an open vertical furnace under a nearly constant heating and cooling rates (5^oC min^{-1}). Due to moister and/or gas surface adsorption, the conductivity of the SHF samples showed an unstable relatively poor initial value at a temperature near room temperature. At higher
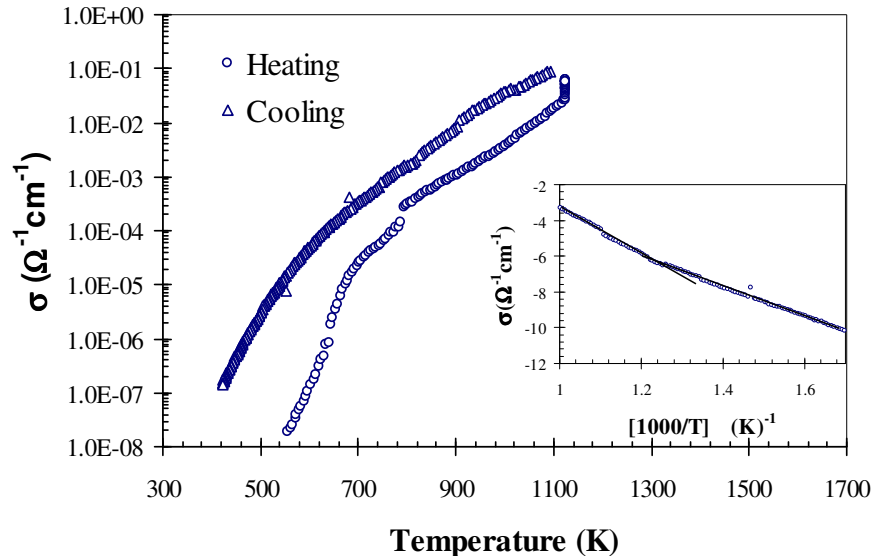
Figure 1. Semi-log plot of the conductivity of SHF nanocrystal compact disks as a function of temperature during heating cooling cycle in air. The inset curve is a straight line fits of the variation of ln(σ) with (1000/T), during cooling, for activation energy calculation.

temperatures, the conductivity increased as the temperature increased, throughout the investigated temperature range, indicating the semiconductor nature of the sample's conductivity. During cooling, the conductivity retains values higher than that obtained during heating; this may be explained by the fact that the conduction in ferrites is a combination of electronic and ionic that is significantly affected by the oxygen vacancies and/or lattice defects within the sample (Patrakeev et al., 2001, 2005, 2004). In other wards, the oxygen absorption/desorption into/from the sample that affects the oxygen stoichiometry, and hence the conductivity, is the reason for the observed irreversible conductivity values of the SHF nanocrystals during heating-cooling measurements.

For semiconductor materials, the variation of conductivity with temperature follows an Arrhenius-like dependence (Patrakeev et al., 2001, 2005, 2004; El-Saadawy, 2000; Seshamma et al., 2006),

$$\sigma = \sigma_0 \exp\left[- E_a / k_B T\right] \qquad (1)$$

Where σ_0 is a constant, E_a is the activation energy for electrical conduction, and k_B is the Boltzmann's constant. The inset of Figure 1 shows the natural log of the measured conductivity as a function of (1000/T) for activation energy determination. It is clear that the conductivity satisfies a broken straight line with a transition temperature ~ 500°C. This trend indicates a charge carrier generation/transportation mechanism at higher temperature that is different from that at lower temperature with activation energies to be 1.06 and 0.72 eV, respectively,

measured during cooling. It is reported that in hexaferrite crystals the conduction is due to electrons at lower temperature whereas at higher temperature it is dominated by ionic hopping mechanism (Patrakeev et al., 2001; El-Saadawy, 2000; Seshamma et al., 2006). Furthermore, SHF is a ferromagnetic with curie transition temperature; the material is transformed from the ferromagnetic phase at lower temperature to a paramagnetic phase at higher temperatures. The Curie point is high enough to coincide with the temperature required to generate oxygen vacancy (El-Saadawy, 2000; Seshamma et al., 2006). The transition not only changes the carrier density due to vacancy generation but also the carrier mobility due to increase in lattice defects and phonon scattering. Thus, the two activation energy straight lines of the conductivity confirm the transition of the SHF nanocrystal compact disks from order ferromagnetic phase, where electronic conduction dominates the carrier transportation/conduction, to the random paramagnetic phase, where ions become more mobile and ionic conduction with higher activation energy dominates the conduction within the sample.

For conductivity dynamics during hydrogen gas flow, the SHF nanocrystal compacts were left at the operating temperature (400 - 600°C) for about 30 min in nitrogen gas atmosphere. Few minutes after switching the nitrogen gas off, hydrogen gas switch is turned on (0.5 L/min) and so is the computerized electric conductivity measurement. Figure (2) shows the variation of the electric conductivity of SHF nanocrystal compacts with time in a hydrogen flow (0.5 L/min) at different temperatures (400 - 600°C). Generally, it is observed that the electric conduc-
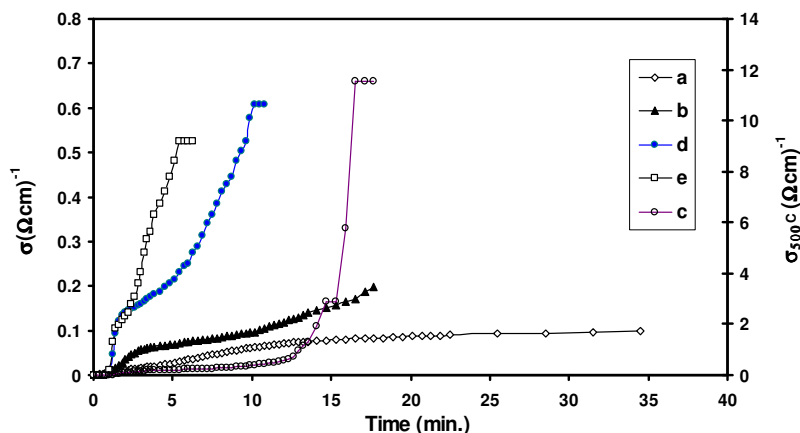
Figure 2. Conductivity transients at various temperatures during hydrogen gas flow of 0.5L min^{-1} at constant pressure at (a) 400°C, (b) 450°C, (c) 500°C, (d) 550°C, (e) 600°C.
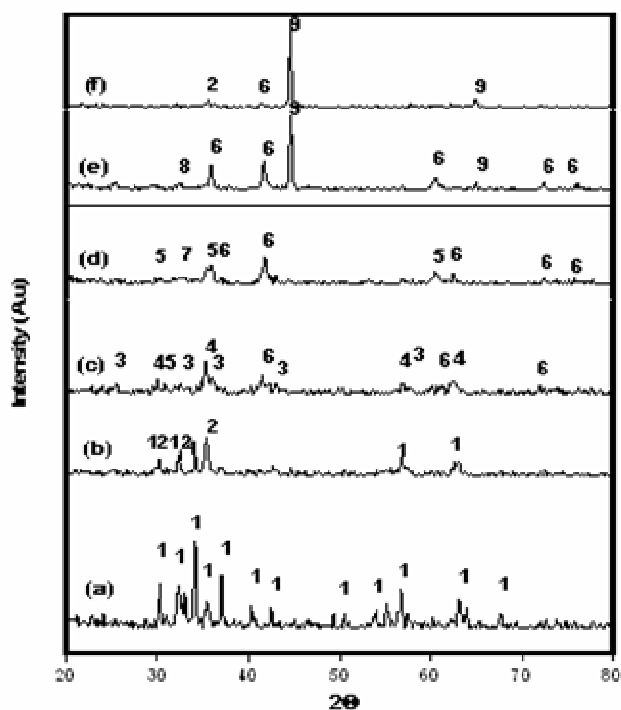
Figure 3. XRD diffractograms of (a) unreduced SHF nanocrystal compacts, and nanocrystals completely reduced at (b) 400°C, (c) 450°C, (d) 500°C, (e) 550°C, (f) 600°C in a hydrogen gas flow. (1) $SrFe_{12}O_{19}$, (2) Fe_2O_3, (3) $Sr_7Fe_{10}O_{22}$, (4) Fe_3O_4, (5) $Fe_{21.34}O_{32}$, (6) FeO, (7) $Sr_4Fe_6O_{13}$, (8) $Sr_2Fe_2O_5$, (9) Fe.

tivity increased by increasing the gas exposure time, which confirms that SHF is an n-type semiconductor and electrons are the majority carriers. During hydrogen exposure, oxygen from the surface as well as from the bulk is removed as water molecules and conducting electrons are lifted behind without molecular orbital to accom-

modate them. These freed electrons are transferred into the conduction band resulting in a decrease in the resistance of the sample and an increase in its electronic conductivity. Had SHF is a p-type or p-type like semiconductor, the sample will have a majority hole charge carriers. As the electron got liberated by the removal of oxygen atoms, a decrease in the conductivity would be observed due to the decrease in the allowed carrier density resulted from the recombination of the liberated electrons with the valance band majority holes, or by being trapped in hole-like localized positive ions. Since this not been the case, the observed trend imply a n-type semiconductor behavior.

By increasing the hydrogen gas exposing time, the reduction extent (percentage) increased producing different phases of strontium–iron oxides, iron oxides and iron metal depending on the operating temperature, as confirmed by ex situ XRD. Formation of different oxide phases and transformation of these oxides from valance state to another may increase the ionic conductivity as well as the electronic conductivity and hence the total conductivity is increased. A complete sample reduction is recognized by minimum resistant readings, while conductivity change with time is an indication of reduction rate. The reduction process is terminated as the conduc-tivity change with time become minimal. It is clear that the time required for complete reduction decreased by increasing reduction temperature from 400 up to 600°C.

The temporal changes of conductivity as well as the formed phases at partial or complete reduction were found to be significantly affected by the operating temperature. Figure 3 shows the XRD patterns of SHF nanocrystal after complete reduction at different temperatures (400 - 600°C). At reduction temperature 400°C, SHF nanocrystal compact disks were partially reduced producing small portions of lower oxides as Fe_2O_3. An exponential increase of the electrical conductivity was observed at the beginning of the reduction process at this temperature,

Table 1. Crystal size and the phase content for completely reduced SHF compacts as obtained from XRD analysis.

Reduction temperature (^{o}C)	phases content	Crystal size (nm)
400	$SrFe_{12}O_{19}$	81.5
	Fe_2O_3	23.3
450	$Fe_{21.4}O_{32}$	18.2
	$Fe_{0.9}O$	13.4
	Fe_3O_4	28.8
	$Sr_7Fe_{10}O_{22}$	30.1
500	$Sr_4Fe_6O_{13}$	62.1
	$Fe_{21.4}O_{32}$	32.2
	FeO	23.7
	Fe metal	43.2
550	Fe metal	98.2
	FeO	36.2
	$Sr_2Fe_2O_3$	31.8
600	Fe metal	104

which may be attributed to the desorption of adsorbed oxygen resulting in an increase in the conduction band electrons by two electron per each desorped atom. After complete oxygen desorption, the surface is reduced and the electrical conductivity is further increased but with a lower rate.

XRD of SHF nanocrystal compact disks reduced at temperatures of 450 and 500°C, (Figure 3), confirms the formation of new oxides of lower oxygen content such as $Fe_{21.4}O_{32}$, $Fe_{0.9}O$, Fe_3O_4, and $Sr_7Fe_{10}O_{22.4}$. Formation of these oxides due to SHF reduction by hydrogen increases the ionic conduction rather than the electronic (34.2 nm) that have a great conductivity compared to its oxides. At higher reduction temperatures (550 and 600°C), the iron oxides and iron metal content increase, peak intensity increased, with increasing crystal sizes as a result of sintering at high reduction temperatures. Table 1 shows the crystal size and the formed phases of completely reduced SHF nanocrystal compact disks as obtained from XRD patterns. The total conductivity is increased with a maximum value lower than that observed at 500°C because of low drift mobility resulted from structural defects occurred at higher reduction temperature. These structural defects were due to the increase in oxygen vacancies and the grain growth after sintering at high reduction temperature. These defects act as scattering and trapping centers (Patrakeev et al., 2001, 2005; Keshmiri et al., 2002; Dawar and Joshi, 1984; Jukichihombo et al., 1990). Similar observation have been reported, where prolonged hydrogenation were found to have negative effects on electrical conductivity (Keshmiri et al., 2002).

Figure 4 shows TEM of the unreduced SHF and SHF nanocrystals after complete reduction in hydrogen envi-

ronment (0.5 L/min.) at the lowest and highest investigated temperatures (400 and 600°C) along with its size distribution histograms and size statistics.

Unreduced SHF nanocrystals were found to have relatively elongated anisotropic polyhedron as well as rounded crystal shapes with larger sizes and size distribution that spans over a wide particle sizes. On the other hand, reduced samples were found to have almost rounded crystal shapes with smaller sizes and narrower size distributions. The average particle size decreased from 88 nm of the unreduced samples to 77 and 61 nm, for samples reduced at 400 and 600°C, respectively. This observation indicates that exposing to hydrogen gas flow modifies the crystal morphology as well as producing crystals with lower sizes, in consistence with previously reported results (Ataie et al., 1996; Ebrahimi et al., 1999).

Sizes calculated from XRD are consistent with those measured by TEM, except for samples with many phase (600°C). TEM images of SHF nanocrystals reduced at 600°C showed a gray and dark crystallite patterns indicating atomic agglomeration and different phase formation in consistent with XRD results.

In order to identify the formed phases during reduction, hydrogen gas is turned off before complete reduction, and partially reduced SHF nanocrystal compacts were sent for ex situ XRD. Figure 5 shows some XRD patterns obtained for partially reduced nanocrystals at different temperatures. It is clear that partial reduction of SHF nanocrystals at temperatures of 400 and 450°C for 18.5 and 7.5 min, respectively, produces no metallic iron or iron oxides phases. Also, no iron metal was formed for SHF nanocrystals partially reduced at 550°C for 3.5 min, however lower oxygen content oxide such as $Sr_2Fe_2O_5$ and Fe_3O_4 magnetite were formed. After longer reduction time, 20 min, FeO, $Sr_2Fe_2O_5$ and iron metal, with larger crystal sizes are formed at that temperature, 550°C. Table 2 shows the crystal size and phase content as obtained from XRD patterns of partially reduced SHF nanocrystal compacts. Partial reduction at 600°C for 3 min shows that iron metal is formed with small percentage with the major products to be Fe_3O_4 and $Sr_2Fe_2O_5$. By increasing the reduction time for 11 min, the formed phases are FeO and Fe metallic nanocrystals.

An important feature characterizing the conductivity-time dependent curves obtained for SHF nanocrystal compact disks, Figure 2, is the change in the conductivity rate as the hydrogen exposing time increase, which is also temperature dependent. In other words, at a given temperature, the obtained curve can be subdivided into regions each of which is characterized by a constant conductivity change rate. As mentioned before the conductivity change rate is a function of the reduction rate and hence is determined by the chemistry of gas solid interaction, which is thermally activated by the operating temperature. For nanocrystals reduced at reduction temperature of 400 ℃, two reduction regions could be identified, whereas those reduced at higher temperatures (500
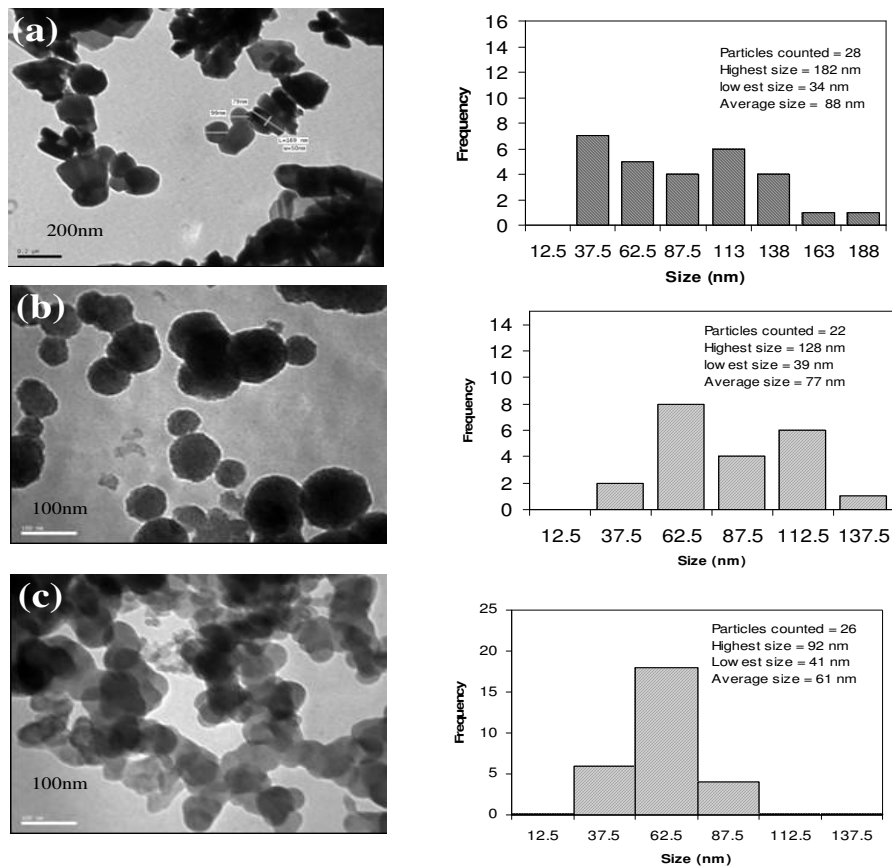
Figure 4. TEM images along with the size distribution and some statistics of (a) unreduced SHF nanocrystals, and nanocrystals reduced at (b) 400°C and (c) 600°C
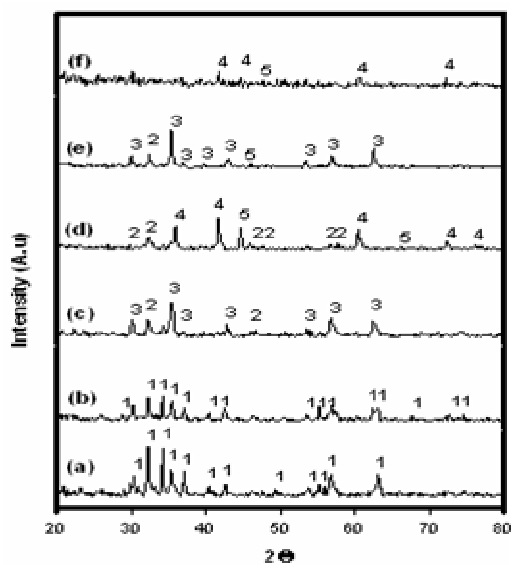
Figure 5. XRD diffractograms of partially reduced SHF nanocrystals reduced at different temperatures: (a) at 400°C for 18.5 min, (b) at 450°C for 7.5 min, (c) 550°C for 3.5 min, (d) at 550°C for 20 min, (e) at 600°C for 3 min, (f) at 600°C for 11min. (1) $SrFe_{12}O_{19}$ (2) $Sr_2Fe_2O_5$ (3) Fe_3O_4 (4) FeO (5) Fe.

- 600°C) showed three regions. These region are consistence with the desorption of the adsorbed oxygen gas at early reduction stage, followed by reduction of the surface layers of the nanocrystals, and finally the bulk interior of the nanocrystals is reduced at longer exposing time (Khedr, 2005; El-Geassy, 2004). Figure 6 shows optical microscope images of partial and complete reduced SHF nanocrystal compacts. Images of partial reduced samples showed layer like structures indicating regions with different oxygen contents and hence reduction process that proceeds from the surface. On the other hand, completely reduced samples or sample reduced for longer times have homogeneous profile images. Because reduction is an energy activated thermodynamic process, bulk reduction is not observed at lower temperature. To determine the rate controlling mechanism at the initial, intermediate and final stages of reduction, the apparent activation energy (E_a) was calculated from Arrhenius equation:

$$Kr = K_0 e^{-Ea/RT} \qquad (2)$$

Where R is the gas constant, T is the absolute temperature, K_0 is the pre-exponential factor and Kr is the rate constant. The apparent activation energy value

Table 2. Crystal size and phase content as obtained from XRD analysis of partially reduced SHF nanocrystal compact disks.

Reduction temperature (°C)	Reduction time (min)	phases content	Crystal size (nm)
400	8.5	$SrFe_{12}O_{19}$	84.2
450	7.5	$SrFe_{12}O_{19}$	69.9
550	3.5	$Sr_2Fe_2O_5$,	40.3
		Fe_3O_4 (magnetite)	132.4
	20	Fe (metal)	88.8
		FeO (wuestite)	35.6
		$Sr_2Fe_2O_5$	113.3
600	3	Fe metal	31.5
		Fe_3O_4 (magnetite)	51.7
		$Sr_2Fe_2O_5$	34.9
	11	FeO (wuestite)	29.4
		Fe (metal)	-
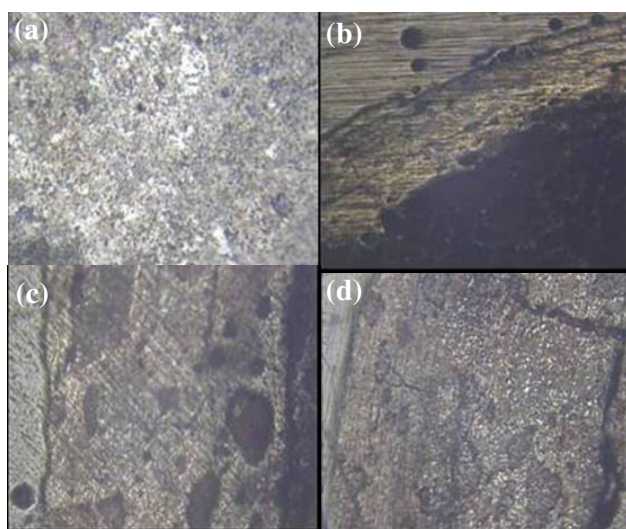
Figure 6. Some photomicrographs of SHF nanocrystals partially and completely reduced in a hydrogen gas flow at different temperatures: (a) partially reduced at 400°C (×400), (b) completely reduced at 400°C (×400), (c) partially reduced at 600°C for 3 min (x100), and (d) partially reduced at 600°C for 11 min (x100).

Table 3. Relationship between activation energy range and the rate controlling step.

Activation energy range Ea (kJ mol^{-1})	Probable rate controlling step
8–16	Gas diffusion
29–42	Combined gas diffusion and interfacial chemical reaction
60–67	Interfacial chemical reaction
>90	Solid-state diffusion

have been calculated by many investigators in order to determine the rate controlling mechanism step. The general ranges of values that have been obtained by Strangway (1964) and recently proved by other studies (El-Geassy et al., 2004; Al-Madfaa et al., 2004; Khedr, 2000) are summarized in Table (3). Therefore, the rate constants for oxygen desorption ($K_{des,}$), surface reduction ($K_{Sred,}$), and bulk reduction (K_{Bred}) are obtained from the slopes of [ln σ versus time straight lines at a given reduction temperature. Utilizing Arrhenius relation and plotting the rate constant as a function of the reduction temperature, the activation energy can be calculated.

Figure 7 shows the Arrhenius plots of K_{des}, K_{Sred}, and K_{Bred} as a function of reduction temperatures. These plots are straight lines with negative slopes. The activation energy value obtained at the initial stages of reduction is found to be 55.5 kJ mol^{-1} indicating a chemical reaction-controlled mechanism. At the intermediate and long hydrogen exposing times the values of activation energy are 40.0 and 44.1 kJ mol^{-1} respectively, which indicate that the rate controlling mechanism is the combined gas diffusion and interfacial chemical reaction. Optical photomicrographs, (Figures 6), showed that compacts are characterized by both open pores at the surface that facilitates the gaseous diffusion and by a dense matrix of SHF supporting the combined mechanism of gaseous diffusion and interfacial chemical reaction. After complete surface reduction, a metal nanocrystals are formed which hinders the gaseous diffusion through the compact bulk and the rate controlling mechanism is thus the gas diffusion mechanism. In other wards, the reduction rate is controlled by the rate of hydrogen diffusion into or oxygen diffusion out of the solid rather than the interfacial gas-solid interaction rate.

Further investigation of nanocrystal reduction was carried out by thermogravimetry. The reduction kinetics was studied by measuring the reduction percentage as a
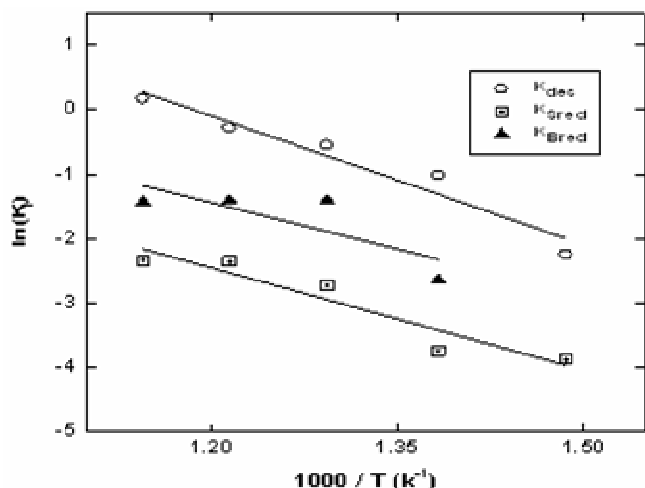
Figure 7. Arrhenius plots of oxygen desorption, surface reduction, and bulk reduction for SHF nanocrystal compact disks reduced at different temperatures.
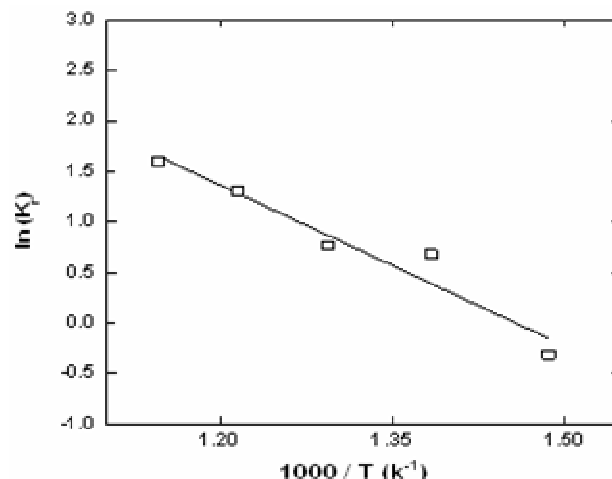
Figure 9. Arrhenius plot of SHF reduction as deduced from thermogravimeric measurements.
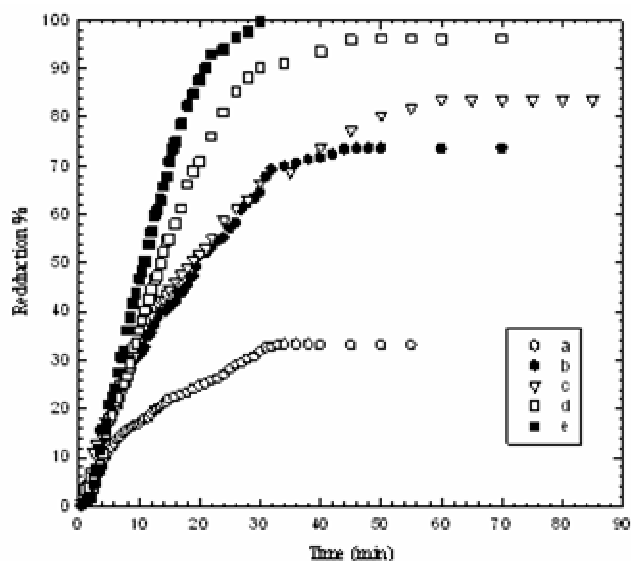
Figure 8. Reduction percentage at various temperature of SHF nanocrystal compact disks during a constant hydrogen gas flow of 0.5 L min^{-1} and at constant pressure at (a) 400°C, (b) 450°C, (c) 500°C, (d) 550°C, (e) 600°C.

a function of the exposing time. A set of dynamic curves similar in methodology to those obtained by dynamic conductivity measurements is obtained and are shown in figure 8. It is clear that SHF nanocrystal compacts continue to lose its oxygen content gradually during hydrogen exposure with a rate (0.5 L/min) that is temperature dependent (400 - 600°C). These results are in consistence with that obtained from in situ dynamic conductivity and ex situ XRD. It also confirms that the total reduction times depends inversely on the reduction tem-

temperature; it is shorter at higher temperature. However, no distinct linear regions could be identified for the oxygen weight loss curves similar to those observed during electrical conductivity measurements. The curves start with nearly exponential weight changes with time, followed by a linear or linear-like region before its monotonic nearly saturated behavior. The slop of the straight line part of the curve can be used to determine the overall rate constant of the reaction process (Strangway, 1964). The straight line relationship of the natural logarithm of the obtained rate constant versus 1000/T K^{-1} gives the activation energy. Figure 9 gives such straight line relationship deduced from the thermogravimetric curves. The slope of this straight line gives the overall activation energy of the reduction process according to the relation in equation (2). The activation energy is 44.1 kJ mol^{-1}, which coincide nicely with the value obtained by dynamic conductivity measurements. It also confirms the process to be of combined gas diffusion and interfacial chemical reaction controlled mechanism.

Summary AND Conclusions

The phase and electrical conductivity dynamics of self-flash combustion SHF nanocrystal compacts were studied in a hydrogen gas flow at atmospheric pressure and at different temperatures. Electric conductivity-temperature dependent measurements of SHF in air showed that the nanocrystal compacts have semiconductor behaviors with transition temperature in conduction that coincide with its magnetic Curie point. Electric conductivity measurements in a hydrogen gas flow showed that the material is n-type with electrons as majority carriers. During hydrogen gas exposure, oxygen from the surface as well as from the bulk of the SHF nanocrystal is removed as water molecules resulting in the formation of different

phases of strontium–iron oxides, iron oxides and iron metal depending on the operating temperature. Formation of different oxide phases and transformation of these oxides from valance state to another increases the ionic conductivity as well as the electronic conductivity and hence the total conductivity is increased.

The temporal changes of conductivity as well as the formed phases at partial and complete reduction were found to be significantly affected by the operating temperature. The total reduction times of the SHF nanocrystals were found to depend inversely on the reduction temperature; it is shorter at higher temperature. Nanocry-stals reduced at higher temperatures showed the formation of metallic iron with increasing sizes responsible for higher electric conductivity during reduction as shown in XRD patterns of partially reduced nanocrystals.

The curve of the conductivity change with time during hydrogen exposure showed three regions consistence with the desorption of the adsorbed oxygen gas at early reduction stage, followed by reduction of the surface layers of the nanocrystals, and finally the bulk interior of the nanocrystals is reduced at longer exposing time. For nanocrystals reduced at reduction temperature of 400°C two reduction regions could be identified, whereas those reduced at higher temperatures showed three regions. Calculating the activation energy for each reduction region indicates that oxygen desorption region follows a chemical reaction controlled mechanism, while surface and bulk reduction regions are of combined gas diffusion and interfacial chemical reaction controlled mechanisms. Thermogravimetry measurements confirmed these activation energies and reduction controlled mechanisms for hydrogen-SHF nanocrystal interaction.

REFERENCES

Adler P (1999). "Charge disproportionation in iron(IV) oxides: electronic properties and magnetism in Sr3Fe2–xTixO7–y annealed at high oxygen pressures. J. Mater. Chem. 9: 471-477.

Al-Madfaa HA, Khader MM (2004). "Microstructure, kinetics and mechanisms of nano-crystalline CuFe2O4 reduction in flowing hydrogen at 300–600°C for the production of metallic nano-wires" Mater. Chemi. and Phys. 86: 180-188.

Ataie A, Heshmati-Manesh S (2001). "Synthesis of ultra-fine particles of strontium hexaferrite by a modified co-precipitation method. J. Eur. Ceram. Soc. 21: 1951.

Ataie A, Ponton CB, Harris IR (1996). "Heat treatment of strontium hexaferrite powder in nitrogen, hydrogen and carbon atmospheres: a novel method of changing the magnetic properties''. J. Mater. Sci. 31: 5521-5527.

Dawar AL, Joshi JC (1984). "Semiconducting transparent thin films: their properties and applications''. J. Mater. Sci. 19: 1-23.

Ebrahimi SAS, Ponton CB, Harris IR (1999). "Characterization and optimization of the coercivity-modifying nitrogenation and re calcination process for strontium hexaferrites powder synthesized conventionally J. Mater. Sci. 34: 35-52.

El-Geassy AA, Nasr MI, Khedr MH, Abdel-Halim KS (2004). "Reduction Behaviour of Iron Ore Fluxed Pellets under Load at 1 023-1 273 K ISIJ Int. 44(3): 462.

El-Saadawy M (2000). "DC conductivity for hexaferrites of the Zn 2-x Cu x Ba 1 Fe 16 O 27 system" J. Magne. Magn. Mater.219: 69-72.

Fu Y, Lin C, Pan K (2003). "Strontium hexaferritespowders prepared by a microwave-induced combustion process and some of their proper-

properties". J. Alloy comp. 349: 228-231.

Gerber R, Atkinson R, Simsa Z (2000). "Magnetism and magneto-optics of hexaferrite layers". J. Magne. Magn. Mater. 175 (2000): 79-89.

Hodges JP, Short S, Jorgensen JD, Xiong X, Dabrowski SM, Mini SM, Kimball CW (2000). "Evolution of Oxygen-Vacancy Ordered Crystal Structures in the Perovskite Series SrnFenO3n−1 (n=2, 4, 8, and ∞), and the Relationship to Electronic and Magnetic Properties. J. Sol. State. Chem.151: 190.

Hong YK, Jung HS, Hur NP, Matar S (1997). "The Effects of Hydrogen Reduction on Magnetic Properties of Barium Ferrite Particles. J. Phys. IV 7(1): 329.

Hwang DC, Yuh-Yuh C (2002). "Synthesis of strontium ferrite nanoparticles by coprecipitation in the presence of polyacrylic acid'' Mater. Res. Bull. 37: 801

Kaura B, Bhata M, Liccib F, Kumarc R, Kulkarnid SD, Joyd PA, Bamzaia KK, Kotrua PN(2006). "Modifications in magnetic anisotropy of M—type strontium hexaferrite crystals by swift heavy ion irradiation" J. Magne. Magn. Mater. 305: 392–402.

Keshmiri SH, Rezaee-Roknabadi M, Ashok S (2002). "A novel technique for increasing electron mobility of indium-tin-oxide transparent conducting films". Thin. Soli. Film. 413: 167-170.

Khedr MH (2000) "Isothermal Reduction Kinetics of Fe2O3 Mixed with 1–10% Cr 2 O 3 at 1173–1473 K". ISIJ Int. 40(4): 309-314.

Khedr MH (2005). "Isothermal reduction kinetics at 900-1100°C of NiFe2O3 sintered at 1000-1200°C. J. Anal. Appl. Pyrol.73 (2005) 123.

Kirchmayr HR (1996). "Permanent magnets and hard magnetic materials". J. Phys. D. Appl. Phys. 29: 2763-2778.

Kitahata S, Kishimoto M (1994). "Magnetic properties of composite Ba-ferrite particles containingα-Fe". IEEE Transactions on Magne. 6: 4107.

Licci F, Renaldi S, Besagni T (1983). "Substrates for epitaxial growth of hexaferrite films". Mater. Let 1(5): 163-165.

Pardavi-Horvath M (2000). "Microwave applications of soft ferrites". J. Magne. Magn. Mater. 215-216, 171-183.

Patrakeev MV, Leonidov IA, Kozhevnikov VL, Kharton VV (2004). "Ion–electron transport in strontium ferrites: relationships with structural features and stability". Soli. Stat. Sci.6: 907–913.

Patrakeev MV, Mitberg EB, Leonidov IA, Kozhevnikov VL (2001). "Electrical characterization of the intergrowth ferrite Sr 4 Fe 6 O 13+ δ" Sol. State. Ioni.139: 325–330.

Patrakeeva MV, Leonidova IA, Kozhevnikova VL, Poeppelmeier KR (2005). "p-Type electron transport in La1– xSrxFeO3– δ at high temperatures". J. Soli. Stat. Chem.178: 921–927.

Prado F, Manthiram A (2001). "Synthesis, Crystal Chemistry, and Electrical and Magnetic Properties of Sr3Fe2–xCoxO7–δ (0≤x≤0.8). J. Solid State. Chem.150: 307-315.

Sankaranarayanan VK, Pant RP, Rastogi AC (2000). "Spray pyrolytic deposition of barium hexaferrite thin films for magnetic recording applications" J. Magne. Magn. Mater. 220: 72-78.

Seshamma NV, Chandra S, Ravinder D (2006). "Thermoelectric power studies of La3+ substituted strontium hexagonal ferrites". J. Alloys. Comp.421: 1–3.

Shilova YA, Patrakeev MV, Mitberg EB, Leonidov IA, Kozhevnikov VL, Poeppelmeier KR (2002). "Order–Disorder Enhanced Oxygen Conductivity and Electron Transport in Ruddlesden–Popper Ferrite-Titanate Sr3Fe2–xTixO6+δ. J. Sol. State. Chem.168: 275.

Strangway PK (1964). M.Sc. Thesis, Toronto University. "The Kinetics of Iron Oxide Reduction" strontium hexaferrites". Tretyakov D: Russian Chemi. Bullet. International. Edition. 54: 75-78.

Zainullina VM, Korotin MA, Kozhevnikov VL (2006). "Electronic structure and properties of strontium ferrite'' Eur. Phys. J. B. 49: 425–431.

Zaitsev DD, Trusov LA, Kazin PE (2005). Synthesis of glass ceramics containing finely dispersed particles of aluminum-doped M-type.